Proceedings World Geothermal Congress 2000
Kyushu - Tohoku, Japan, May 28 - June 10, 2000

AN ANALYSIS ON THERMODYNAMIC PROPERTIES OF STEAM IN SUBSURFACE POROUS-PERMEABLE HORIZONS OF HYDROTHERMAL SYSTEMS

Giuseppe Natale[1] and Luca Sgheri[2]
[1]Laboratory for Earthquake Chemistry, Graduate School of Science, University of Tokyo
7-3-1 Hongo, Bunkyo-ku, Tokyo 113-0033, Japan
[2]Istituto Analisi Globale e Applicazioni, CNR, Via S. Marta 13/A, 50139 Firenze, Italia

Key words: Hydrothermal systems. Dry steam convection

ABSTRACT
The present model analyses thermodynamic properties of steam which separates from a water body in the proximity of the top of reservoir in the subsurface of a hydrothermal system. Starting with the continuity equation, Darcy's law and the fluid-rock energy equation in the one-dimensional case, we define two coupled non-linear parabolic equations expressed in terms of fluid-rock temperature $T(z)$ and fluid density $\rho_f(z)$. The steady state case is examined and it is reduced to a third order non-linear ordinary differential equation in $y(z)=\rho_f(z)T(z)$. This equation is then solved numerically using an implicit scheme. The mathematical solutions exhibit stable or unstable behaviour of the thermo-dynamic properties of steam depending on the initial conditions which may occur at depth in the vicinity of the top of the reservoir and in particular on the value of the parameter $\alpha=\rho_f\partial_z(\rho_f T)\equiv\rho_f\partial_z P/R$, where R is the gas constant and P the added pore fluid pressure over the hydrostatic value. A theoretical tool is thus supplied, for instance for the management of dry steam producing geothermal systems.

1. INTRODUCTION

The modelling of water circulation through hydrothermal systems has been extensively investigated for geothermal applications, mainly to understand how hydrothermal systems can form and persist within the Earth's crust (see for example, Lapwood, 1948; Goguel, 1953; Donaldson, 1970). In particular, it was found that aquifers are the domain of " water circular convection" as long as the so-called overlying "caprock", which is characterised by a very small or nil permeability value, exists at depth. Moreover, the observation of steam emissions at the surface made some investigators think that subsurface feeding aquifers are the site of water circulation in its gaseous state. A consideration which brought in the definition of "vapour-dominated" hydrothermal systems as opposed to the "liquid-dominated" ones when hot liquid water emissions were observed (see for example, White *et al*., 1971). In contrast to this "static definition" of hydrothermal systems, a study which was based upon a thermodynamic perspective (Facca and Tonani, 1961) envisaged a "dynamic definition" of hydrothermal systems. In this connection, water in aquifers circulates in its liquid state and steam can be generated either in the proximity of the aquifer-caprock boundary or at a certain level within fractured portions of the caprock, depending on both local geothermobaric conditions and fluid-dynamic regimes of water.

In this paper we focus the attention upon the thermodynamic behaviour of steam which separates from a water body at depth and we analyse its stable and unstable behaviour depending on the value of $\alpha=\rho_f\partial_z(\rho_f T)\equiv\rho_f\partial_z P/R$, where R is the gas constant and P the added pore fluid pressure over the hydrostatic value $\rho_f(z)$ the fluid density and $T(z)$ the fluid-rock temperature.

The present model is based upon a set of two coupled non-linear parabolic equations which are expressed in terms of $\rho_f(z)$ $T(z)$ variables. The steady state case is analysed through the definition of a third order non-linear ordinary differential equation in the variable $y(z)=\rho_f(z)T(z)$.

We adopt the Berea sandstone as the rock type constituting the porous-permeable horizon and steam in its supercritical state ($T_0=400^oC$ and $P_0=3\cdot10^7 Pa$) moving through the overburden rock.

2. BRIEF LAYOUT OF HYDROTHERMAL SYSTEMS

Hydrothermal systems may be regarded as the result of a set of possibly interacting reservoirs (Fig. 1) (Natale *et al*., 1999) defined as just a few subsurface bodies, respectively subsurface gas bodies and subsurface water bodies, which interact with both the Earth's atmosphere and a deep non-observable reservoir, in general related to a magma body. These reservoirs acan be considered homogeneous bodies both chemically and physically, with frontiers corresponding to portions of the crust throughout which interactions may occur in terms of diffusive and convective transport mechanisms.

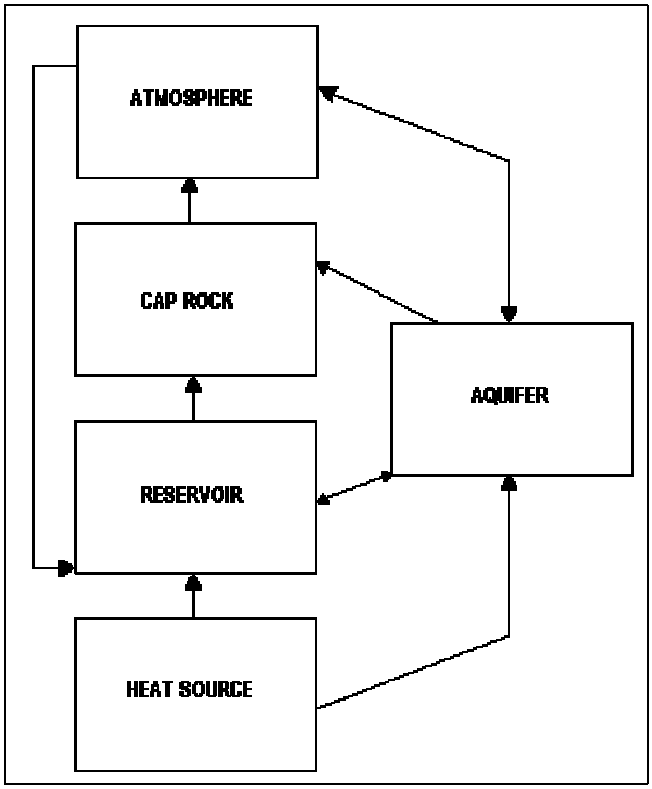

Figure 1. Block diagram: conceptual representation of a hydrothermal system conceived in terms of a set of interacting reservoirs

We here ignore processes connected to diffusive interactions between the reservoirs and then focus the attention on the

convective interaction and in particular on the thermo-dynamic properties of steam which separates from a water body in the proximity of the top of a reservoir and which can migrate through fractures or pipes eventually existing within the overlying caprock. The porous-permeable horizon is supposed to be chemically and mechanically inert, isotropic and homogeneous, i.e., to have constant values of permeability, porosity, thermal capacity, thermal conductivity and density during the process (Fig. 2). Furthermore, the model is one-dimensional inasmuch as we are interested on the physical nature of the process rather than on its spatial structure.
ter-saturated porous-permeable horizon) and overlying cap rock

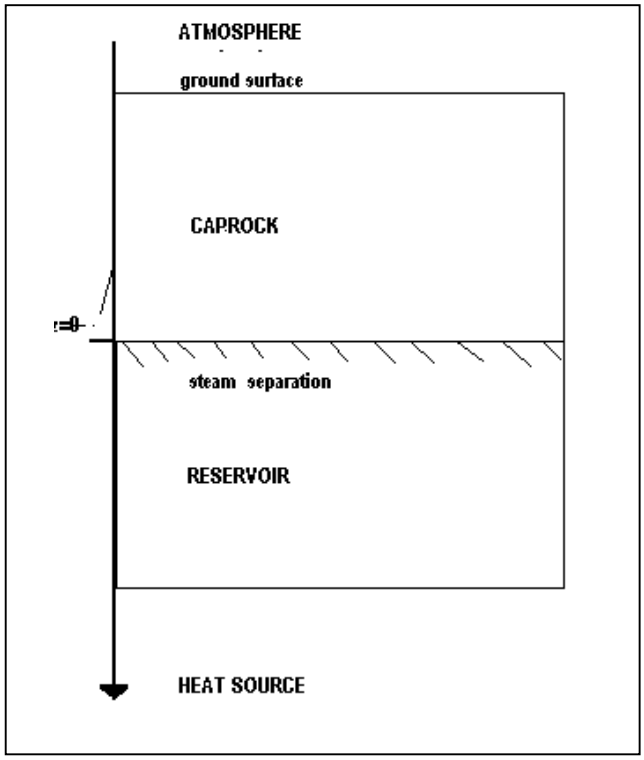

Figure 2. Aquifer (water-saturated porous-permeable horizon) and overlying cap rock.

3. FUNDAMENTAL EQUATIONS

Let us define the fundamental fluid-dynamic equations over a representative elementary volume within the porous-permeable horizon of Figure 1.

3.1 Continuity equation

$$\frac{\partial(\rho_f)}{\partial t}+\frac{\partial(\rho_f v_{f_z})}{\partial z}=0 \tag{1}$$

where ρ_f and v_{f_z} are the density and the velocity of the fluid, t the time and z the space coordinates (Table 1).

3.2 Darcy's law

$$v_{D_z}=\phi v_{f_z}=-\frac{K_f}{\mu}\frac{\partial P}{\partial z} \tag{2}$$

where inertia and buoyancy terms are neglected. In equation (2) K_f is the permeability of the rock, ϕ its porosity, μ the fluid viscosity and P the added pore fluid pressure onto the equilibrium hydraulic pressure.

3.3 Ideal gas state equation

The thermodynamic behaviour of water is simplified by the ideal gas state equation:

$$P=\rho_f RT \tag{3}$$

where R is the gas constant and T the temperature.

3.4 Fluid-rock energy equation

Under the assumption that the fluid and the overburden rock are in local thermal equilibrium, the energetic contributions respectively due to the fluid and the rock can be simply added up. Thus, the energy equation can be written as follows (Natale, 1998, and bibliography therein):

$$\frac{\partial T}{\partial t}-K_1\frac{\partial^2 T}{\partial z^2}-K_2\frac{\partial P}{\partial z}\frac{\partial T}{\partial z}-K_3T\frac{\partial^2 P}{\partial z^2}-K_4\left(\frac{\partial P}{\partial z}\right)^2=0 \tag{4}$$

where again T is the fluid-rock temperature, K_1 is the average thermal diffusivity due to diffusion controlling diffusive thermal energy exchanges, K_2 and K_3 the average thermal diffusivity due to convection controlling convective thermal energy exchanges and finally K_4 the average dissipative diffusivity due to fluid-rock friction controlling thermal energy generation.

4. COUPLED NON-LINEAR PARABOLIC EQUATIONS

Substituting equation (2) into (1) above, it yields:

$$\frac{\partial \rho_f}{\partial t}-\frac{K_f}{\phi\mu}\frac{\partial}{\partial z}\left(\rho_f\frac{\partial P}{\partial z}\right)=0 \tag{5}$$

and by inserting equation (3) into (5) the first non-linear equation is derived:

$$\frac{\partial \rho_f}{\partial t}-K_2^I\frac{\partial}{\partial z}\left[\rho_f\frac{\partial(\rho_f T)}{\partial z}\right]=0 \tag{6}$$

where $K_2^I=RK_2$.

The other equation to be associated to (6) above may be derived by inserting equation (3) into (4):

$$\frac{\partial T}{\partial t}-K_1\frac{\partial^2 T}{\partial z^2}-K_2^I\frac{\partial(\rho_f T)}{\partial z}\frac{\partial T}{\partial z}-K_3^I T\frac{\partial^2(\rho_f T)}{\partial z^2}-K_4^I\left[\frac{\partial(\rho_f T)}{\partial z}\right]^2=0 \tag{7}$$

where now $K_2^I=RK_2$, $K_3^I=RK_3$, $K_4^I=R^2K_4$ (Table 1).

The coupled equations (6) and (7) may be solved with appropriate conditions at $z=0$. As in principle $\rho_f(0,t)$, $\partial\rho_f(0,t)/\partial z$, $T(0,t)$, $\partial T(0,t)/\partial z$ at a given depth can be either hypothesised in the proximity of the top of the reservoir of Figure 2 or directly measured at the wellhead if a borehole exists, this leads to a class of mathematical problems known as non characteristic Cauchy problem for parabolic equations. This class of problems is difficult to solve as they lack the continuity with respect to the initial data. In other

words there exist two sets of initial data $u_1(t=0)$ and $u_2(t=0)$ such that $\|u_1(t=0)-u_2(t=0)\| \approx \varepsilon$, but

$\|u_1(t)-u_2(t)\| \approx \varepsilon e^{at}$ with $a>0$. The mathematical literature is extensive, see for example the book by Beck et al. (1985).

In order to check the behaviour of the model, in this paper the steady state case is now analysed in detail in the following sections.

5. REDUCTION TO THE STEADY STATE CASE AND INITIAL CONDITIONS

Under steady state conditions equations (6) and (7) become:

$$\frac{\partial}{\partial z}\left[\rho_f \frac{\partial(\rho_f T)}{\partial z}\right]=0 \tag{8}$$

$$K_1\frac{\partial^2 T}{\partial z^2}+K_2^I\frac{\partial(\rho_f T)}{\partial z}\frac{\partial T}{\partial z}+K_3^I T\frac{\partial^2(\rho_f T)}{\partial z^2} + K_4^I\left[\frac{\partial(\rho_f T)}{\partial z}\right]^2=0 \tag{9}$$

which can be solved by using the following initial conditions at $z=0$ (Table 2):

$$T\big|_{z=0}=T_0 \quad \left.\frac{\partial T}{\partial z}\right|_{z=0}=T_0^I \quad \rho_f\big|_{z=0}=\rho_{f_0} \quad \left.\frac{\partial \rho_f}{\partial z}\right|_{z=0}=\rho_{f_0}^I \tag{10}$$

Moreover, by integrating (8) it gives the expression:

$$\rho_f\frac{\partial(\rho_f T)}{\partial z}=const.\equiv\alpha \tag{11}$$

which allows one to replace one of the initial conditions (10) by assigning the value of α. In particular, setting $z=0$ in (11) above it yields:

$$\rho_{f_0}\left(\rho_{f_0}T_0^I+\rho_{f_0}^I T_0\right)=\alpha$$

6. FLUID AT REST. $\alpha=0$ AND NO ADDED PORE FLUID PRESSURE

The system (8)-(9) has some elementary solutions when $\alpha=0$, entailing that the fluid is at rest in the light of (11) and (3). In fact, remembering that $\alpha=\rho_f\partial_z(\rho_f T)=\rho_f\partial_z P/R=0$, only the pore fluid pressure gradient over the hydrostatic value $\partial_z P$ can be nil. In this case $\rho_f(z)T(z)=\rho_{f_0}T_0$, so that from (8) it follows that $\partial_{zz}T(z)=0$ yielding a linear function governing the temperature distribution along the direction z:

$$T(z)=T_0^I z+T_0 \tag{12}$$

Expression (12) above is thus representative of a conductive regime controlling the associated thermal energy migration with a corresponding fluid density profile along z following a hyperbolic law of the form:

$$\rho_f(z)=\frac{\rho_{f_0}T_0}{T_0^I z+T_0} \tag{13}$$

7. FLUID IN MOTION. $\alpha\neq0$ AND ADDED PORE FLUID PRESSURE: CONVECTIVE REGIME

When $\alpha\neq0$ also $\partial_z P\neq0$ and steam moves. Nevertheless, there are no solutions in closed analytical form of the system (8)-(9) in terms of fluid density and fluid-rock temperature fields in the convective case. Let us then reformulate the problem (8)-(9) by introducing the new variable $y(z)=\rho_f(z)T(z)$. In this case $\alpha T(z)=y(z)y^I(z)$ and the system (8)-(9) can be rewritten in terms of a third order non-linear ordinary differential equation as follows:

$$K_1 y^{III}y+\left(K_2^I+K_3^I\right)yy^I y^{II}+K_2^I\left(y^I\right)^3+\alpha K_4^I\left(y^I\right)^2 +3K_3^I y^I y^{II}=0 \tag{14}$$

with initial conditions:

$$y(0)=\rho_{f_0}T_0 \quad y^I(0)=\frac{\alpha}{\rho_{f_0}} \quad y^{II}(0)=\frac{\alpha T_0^I}{\rho_{f_0}T_0}-\frac{\alpha^2}{\rho_{f_0}^3 T_0} \tag{15}$$

derived from (10). The fourth initial condition is the value of the parameter α.

With regards to equation (14) above, the mathematical theory of ordinary differential equations guarantees the existence and uniqueness of solutions as long as $y(z)$ remains limited and bounded away from 0. The solutions of (14) are also continuous with respect to the parameter α. If $\alpha=0$, then $y(z)=const.$ and thus once again (12) and (13) are obtained.

As for $\alpha\neq0$ there are no solutions in closed analytical form, the solution of equation (14) can be approximated with a polynomial using the series method of solution. This approximation is meaningful for small values of z and it may be used to show the influence of non-zero α values. Let $T_0^I=-w\alpha$. A direct calculation shows that plugging in the numerical values of K_i at least for $n\leq200$:

$$y(z)=y(0)+\sum_{i=1}^{n}p_i(w)(\alpha z)^i+r_n(z) \tag{16}$$

with $p_i(w)=(-1)^{i-1}\sum_{j=0}^{i-1}p_{ij}w^j$, with $p_{ij}>0, \forall j<i, i\leq n$.

it follows that when $\alpha<0$ and $w>0$ the first 200 derivatives of $y(z)$ are negative. As an example, the series solution when $\alpha=-1$, $w=1$ is shown in Appendix. This suggests that the mathematical solution may tend towards zero for finite values of z_0. The larger the $|\alpha|$, the sooner this happens. Of course this is not a mathematical proof, just a hint on what is expected when the system is solved numerically.

The ordinary differential equation (14) can be solved numerically using both an implicit high order Adams-Moulton

scheme and a backward differentiation formula of order 4, with similar results. The calculations are carried out in double precision on a PC running *Linux* and *gcc*. A high order series solution is used to check the numerical approximation. Figure 3 shows the case $\alpha < 0$ and $w > 0$, when all the coefficients of the series are negative and Figure 4 shows the case $\alpha > 0$ and $w > 0$ where the coefficients have alternating signs. Two polynomials (one with odd degree and one with even degree) are shown in solid line. Note that there is an almost perfect correspondence between the numerical and the series solution, up to a value z_0 (which depends on the degree of the polynomial) where the series solution diverges consistently with the sign of the leading coefficient.

The behaviour of the solution for $\alpha < 0$ is confirmed, as shown in Figures 5 and 6.

8. DISCUSSIONS AND CONCLUSIONS

In this paper we supply a theoretical tool to describe thermo-dynamic properties of steam which separates from a water body in the vicinity of the top of a reservoir of a hydrothermal system (Fig. 2). We study the fluid-rock temperature and the fluid density distribution as steam circulates in steady state conditions. Figures 7-14 show the numerical results. It should be noted that no solution of (14) may have a flex with horizontal tangent, unless it is the null solution. From the numerical results it seems that both $\rho_f(z)$ and $T(z)$ maintain the initial concavity (or convexity), as shown in figures 7 and 8, where α_0 and α_1 are chosen in such a way that $T^{II}(0)$ and $\rho_f^{II}(0)$ are 0. In figures 9-14 the behaviour of $\rho_f(z)$ and $T(z)$ is shown for different values of α and T_0^I. Physical considerations suggest that the gas temperature should increase with depth z. If the model is fed with a negative initial gradient of temperature, the equation reverse the sign of $T^I(z)$ according to the physical expectations. This paper can for instance supply complementary information for the management of dry steam producing geothermal fields. In fact, the thermo-dynamic properties which the present model hypothesises regarding steam separating from its liquid at the top of a reservoir may be useful to understand the behaviour of fluid density and fluid temperature fields in the proximity of a wellhead. Further development of the present model will entail the transient case which may correspond to the case when a borehole is drilled up and, as a consequence, the top of the reservoir in perturbed from its steady condition in the fluid circulation.

ACKNOWLEDGEMENTS

We thank Hisao Fujita Yashima for his very useful suggestions and Pedro Hernández for support.

APPENDIX

The symbolic package Maple has been used to calculate a series solution of the ordinary differential equation (14). This has been useful to check the behaviour of the numerical solution. In particular, the series solution when $\alpha < 0$ and $T_0^I > 0$ has all first 200 coefficient negative.

As an example, when $\alpha = -1$, $T_0^I = 1$, the series solution of order 30 is:

$$
\begin{aligned}
y(z) = {} & 242280.0 - 0.002777777778\, z - 0.000002063743842\, z^2 \\
& - 0.0000009618510457\, z^3 - 0.0000003365754500\, z^4 \\
& - 0.00000009442058170\, z^5 - 0.00000002216643515\, z^6 \\
& - 0.000000004497539840\, z^7 - 0.000000000813898709\, z^8 \\
& - 0.000000001340900087\, z^9 - 2.103127218\, 10^{-11}\, z^{10} \\
& - 3.263068688\, 10^{-12}\, z^{11} - 5.205229790\, 10^{-13}\, z^{12} \\
& - 8.706185285\, 10^{-14}\, z^{13} - 1.516992646\, 10^{-14}\, z^{14} \\
& - 2.696823576\, 10^{-15}\, z^{15} - 4.800709379\, 10^{-16}\, z^{16} \\
& - 8.478879141\, 10^{-17}\, z^{17} - 1.484859697\, 10^{-17}\, z^{18} \\
& - 2.589263753\, 10^{-18}\, z^{19} - 4.519788555\, 10^{-19}\, z^{20} \\
& - 7.928002876\, 10^{-20}\, z^{21} - 1.399124240\, 10^{-20}\, z^{22} \\
& - 2.482002294\, 10^{-21}\, z^{23} - 4.417551204\, 10^{-22}\, z^{24} \\
& - 7.874769036\, 10^{-23}\, z^{25} - 1.404555919\, 10^{-23}\, z^{26} \\
& - 2.506096904\, 10^{-24}\, z^{27} - 4.474505318\, 10^{-25}\, z^{28} \\
& - 7.997775590\, 10^{-26}\, z^{29} - 1.43153087\, 10^{-26}\, z^{30} + O(z^{31})
\end{aligned}
$$

REFERENCES

Beck J.V., Blackwell B. and St. Clair C.R. Jr. (1985). *Inverse Heat Conduction* (J. Wiley & Sons, New York 1985).

Donaldson, I.G. (1970). The simulation of geothermal systems with a simple convective model, *Geothermics* vol.2/1(2), 649-654.

Facca F. and Tonani F. (1961). Natural steam geology and geochemistry. *Proceedings U.N. Rome Conference on New Sources of Energy*, vol.2, 271-293.

Goguel, J. (1953). Le regime thermique de l'eau souterraine. *Annales des Mines*, vol.10, 3-31.

Lapwood, E.R. (1948). Convection of a fluid in a porous medium. *Proc. Cambridge Phil.Soc.*, vol.44, 508-517.

Natale, G. (1998). The effect of fluid thermal expansivity on thermo-mechanical solitary shock waves in the underground of volcanic domains. *Pure Appl. Geophys.*, vol.152, 193-211.

Natale, G., Salusti, E. and Tonani, F. (1999). Management of dry steam geothermal fields and volcanic explosion forecast: (T,P) solitary waves, a new potential source of significant information. *Proceedings 24th Workshop on Geothermal Reservoir Engineering*, Stanford University, California, Jan. 25-27.

White, D.E., Muffler, L.J.P., and Truesdell, A.H. (1971). Vapor-dominated hydrothermal systems compared with hot-water systems. *Econ. Geol.*, vol.66, 75-87.

K_f	$1.9\cdot10^{-13}$	m^2
ϕ	0.19	
K_T	3	$J\cdot m^{-1}\cdot K^{-1}\cdot s^{-1}$
μ	$8\cdot10^{-5}$	$Pa\cdot s$
ρ_m	$2.2\cdot10^{3}$	$Kg\cdot m^{3}$
ρ_f	$3.6\cdot10^{2}$	$Kg\cdot m^{3}$
c_m	10^{3}	$J\cdot Kg^{-1}\cdot K^{-1}$
c_{v_f}	$2.1\cdot10^{3}$	$J\cdot Kg^{-1}\cdot K^{-1}$
R	$4.61\cdot10^{2}$	$J\cdot Kg^{-1}\cdot K^{-1}$
K_1	$1.13\cdot10^{-6}$	$m^2\cdot s^{-1}$
K_2^I	$5.8\cdot10^{-6}$	$J\cdot m^2\cdot Pa^{-1}\cdot Kg^{-1}\cdot K^{-1}\cdot s^{-1}$
K_3^I	$5.63\cdot10^{-4}$	$J\cdot m^2\cdot Pa^{-1}\cdot Kg^{-1}\cdot K^{-1}\cdot s^{-1}$
K_4^I	$2.96\cdot10^{-10}$	$J\cdot m^5\cdot Pa^{-1}\cdot Kg^{-2}\cdot K^{-1}\cdot s^{-1}$

K_f: permeability, ϕ: porosity, K_T: average thermal conductivity, μ: viscosity, ρ_m: medium density, ρ_f: fluid density, c_m: medium thermal capacity, c_{v_f}: fluid thermal capacity at constant volume, R: gas constant, K_1: initial average thermal diffusivity due to diffusion, K_2^I, K_3^I: initial average thermal diffusivity due to convection, K_4^I: initial average dissipative diffusivity due to fluid-medium friction,

Table 1. Definition and values of parameters for the Berea Sandstone saturated with steam at $T_0 = 400^o C$ and $P_0 = 3\cdot10^7 Pa$ at $z = 0$

T_0	673	K
P_0	$3\cdot10^{7}$	Pa
ρ_{f_0}	$3.6\cdot10^{2}$	$Kg\cdot m^{-3}$
$\partial T/\partial z\big\vert_{z=0}$	$\pm2\cdot10^{-2}$	$K\cdot m^{-1}$
$\partial\rho_{f_0}/\partial z\big\vert_{z=0}$	$\pm2\cdot10^{-2}$	$Kg\cdot m^{-4}$
$v_{D_z}\big\vert_{z=0}$	$7.9\cdot10^{-6}$	$m\cdot s^{-1}$
α	$\pm7.5\cdot10^{3}$	$Kg^2\cdot m^{-7}\cdot K$

T_0: initial fluid-medium temperature, P_0: initial fluid pressure, ρ_{f_0}: initial fluid density, $\partial T/\partial z\big\vert_{z=0}$: initial vertical temperature gradient, $\partial\rho_{f_0}/\partial z\big\vert_{z=0}$: initial vertical density gradient, $v_{D_z}\big\vert_{z=0}$: initial vertical Darcy's velocity

Table 2. Values of the initial conditions.

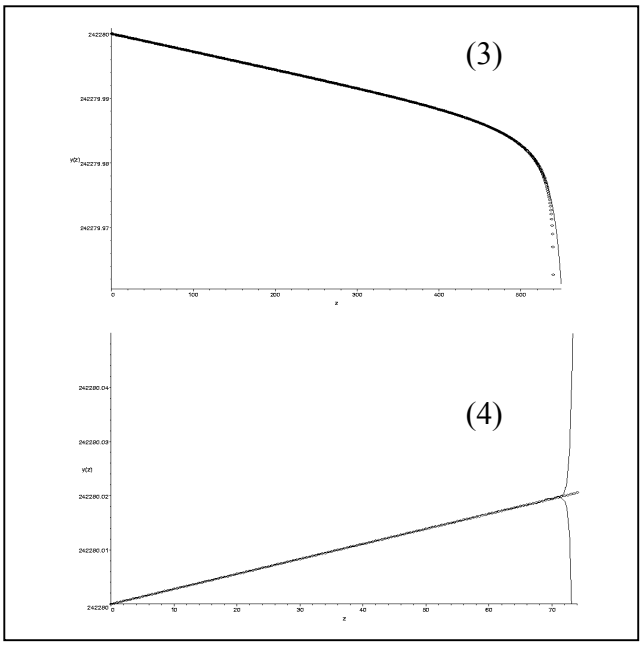

Figures 3-4. Numerical (dotted) and symbolic (solid) approximations to solution of (14); in the case $\alpha < 0$ the coefficient of the series have all the same (negative) sign, in particular here $\alpha = -0.01$, $T_0^I = 0.01$ and polinomial has order 100 (Fig. 3). In the case $\alpha > 0$ the coefficient of the series have alternative sign , two polinomial (begree 200 and 201) are shown with $\alpha = 0.1$, (Fig. 4).

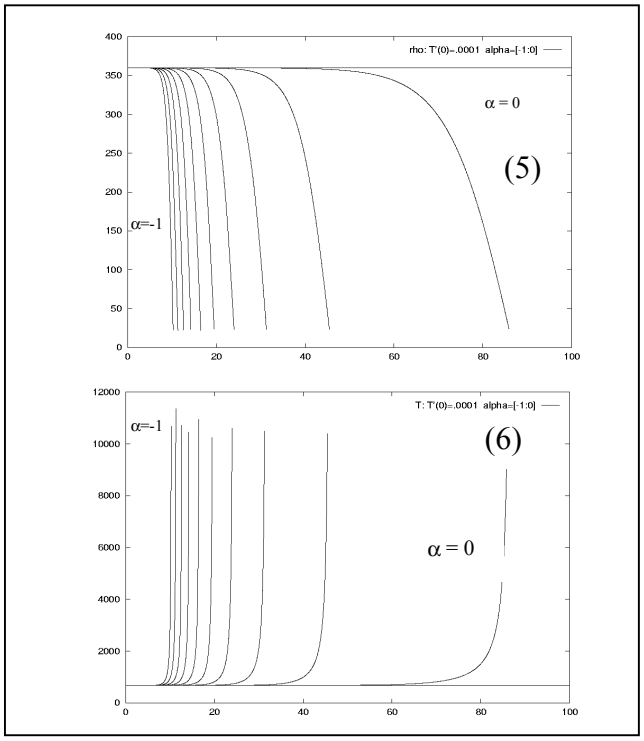

Figures 5-6. Case $\alpha < 0$, graphs $\rho_{f(z)}$ versus z (Fig. 5) and $T(z)$ versus z (Fig. 6), the solution diverges for finite.

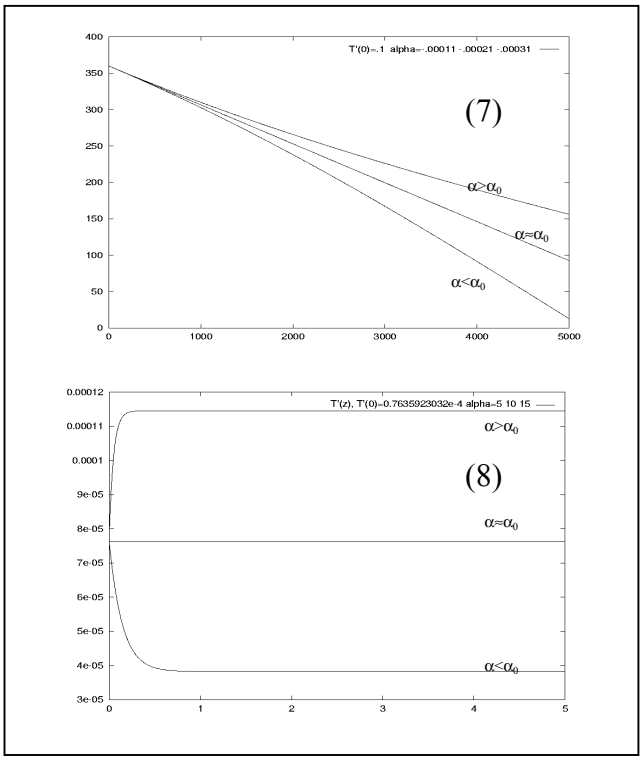

Figures 7-8. Case $\alpha \approx 0$ such that $\rho_f^{II}(0) = 0$ and $T^{II}(0) = 0$, graphs $\rho_{f(z)}$ versus z (Fig. 7) and $T^I(z)$ versus z (Fig. 8).

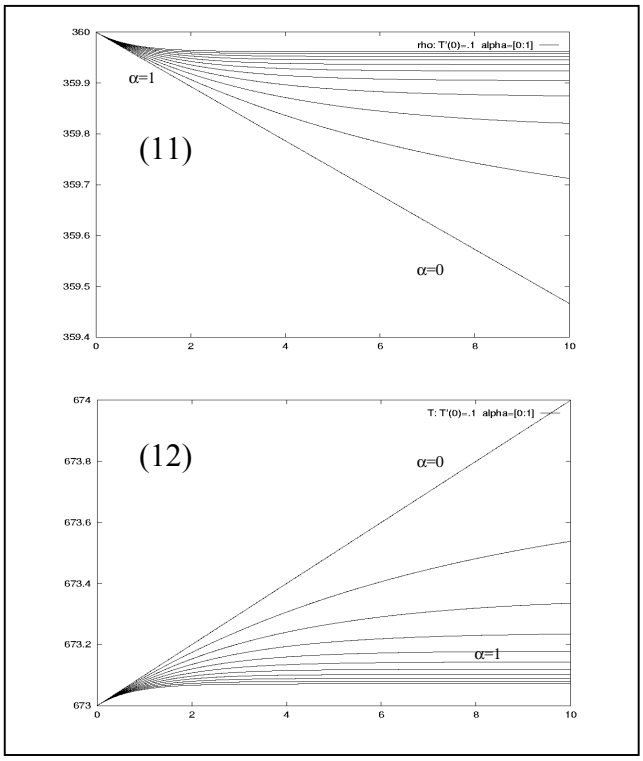

Figures 11-12. Case $\alpha > 0$ and small and $T_0^I > 0$, graphs $\rho_{f(z)}$ versus z (Fig. 11) and $T(z)$ versus z (Fig. 12).

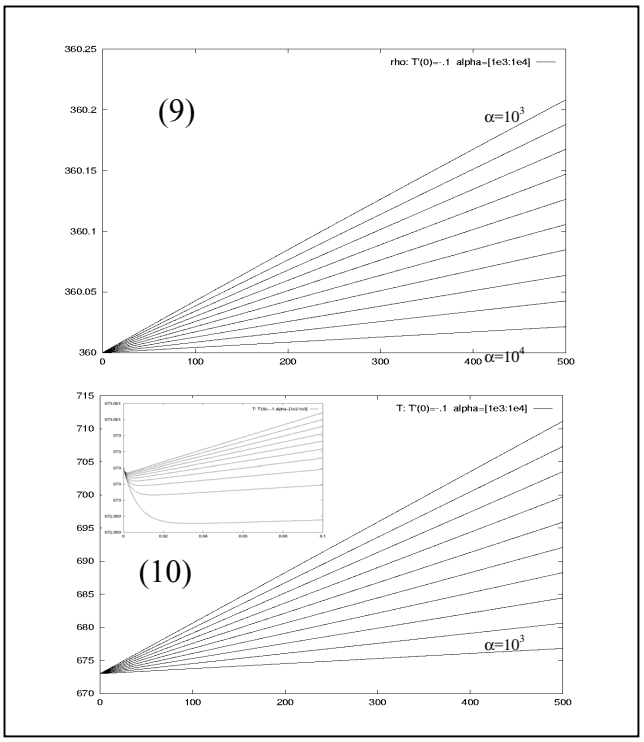

Figures 9-10. Case $\alpha > 0$ and $T_0^I < 0$, graphs $\rho_{f(z)}$ versus z (Fig.9) and $T^I(z)$ versus z (Fig. 10).

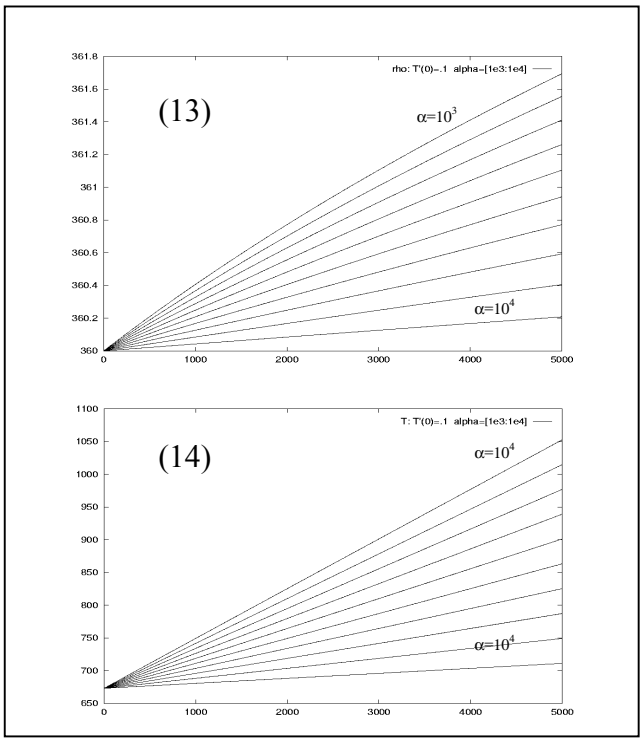

Figures 13-14. Case $\alpha > 0$ and large and $T_0^I > 0$, graphs $\rho_{f(z)}$ versus z (Fig. 13) and $T(z)$ versus z (Fig. 14).